

# **Sensing defects during directed-energy additive manufacturing of metal parts using optical emissions spectroscopy**

A. R. Nassar\*, T. J. Spurgeon\*, and E. W. Reutzel\*

\* Applied Research Laboratory at the Pennsylvania State University,  
University Park, PA 16802

REVIEWED

## **Abstract**

Critical components produced via additive manufacturing must be free of unwanted defects. While defects may be detectable after deposition using nondestructive testing techniques, detecting defects during the deposition process offers many benefits: it may enable users to interrupt deposition to repair the part, or to abort deposition to minimize further loss of time and material. Here, we present a method for real-time defect detection during directed-energy additive manufacturing of metals. The method utilized optical emission spectroscopy and a custom-built data acquisition and control infrastructure. It was implemented on a LENS MR-7 machine, and employed during manufacturing of Ti-6Al-4V components in which defects were intentionally introduced. Emission spectra were correlated with defect locations, determined via computed tomography and metallographic cross-sectioning. Preliminary results indicated that defect formation was correlated with atomic titanium (Ti I) and Vanadium (V I) emissions and that measurement of the line-to-continuum ratio for line emissions could be used for defect detection. Based on these findings, sensing strategies for defect detection and, potentially, in-situ-defect repair may be realizable.

## **1. Introduction**

Additive manufacturing (AM) has emerged as a potentially-transformative technology. However, a key obstacle to adoption of AM as a means to produce components for critical applications is qualification and certification. This is particularly true for manufacturing of metal components. Additively-manufactured, metal components are typically fabricated through powder-bed, powder-blown, or wire-based processes, each of which requires melting and solidification of many individual tracks using a laser or electron beam. During processing, defects can result from improper parameter selection, melt pool instability, greater-than-predicted thermal deformation, environmental or process anomalies (such as gas contamination, a damaged recoater blade, or a clogged powder nozzle), energy source fluctuations, and other machine malfunctions. Monitoring AM processes for such in-process errors is vital to component and process qualification.

Researchers have developed numerous strategies to perform in-process monitoring for metal AM. Broadly, in-process signals can be classified in three categories: beam characteristics, worktable/motion characteristics, and process characteristics [1]. Specifically, researchers have monitored laser/e-beam parameters, melt pool metrics, part temperature, feed material or powder

bed, geometry, and optical emissions during processing. See [1]–[4] for reviews on in-process monitoring for laser-materials processing and AM.

A common strategy is sensing and control of melt-pool size [5]–[9] or temperature [10], [11]. Other efforts have attempted to maintain a constant layer build height by directly sensing build height and adjusting processing head position [12], processing speed [13], [14], filler material feed rate [15], or laser power [16]. Recently, researchers have also investigated the use of optical emission spectroscopy (OES) for monitoring of AM processes [17]–[19].

Optical emission spectroscopy has long been used to better understand physical mechanisms and to monitor conditions during laser-materials processing. In CO<sub>2</sub> laser welding of AISI 304 stainless steel, Ancona et al. [20] used in-process OES to measure the excitation temperatures of iron, chromium, and magnesium vapors and found that welding defects correlated with fluctuations in one or more species temperature. OES has also been used to study the effect of gas shielding [21], vaporization [22], [23], and weld quality [24] during laser welding. It has also been used to study processing regimes and oxidation during laser nitriding of titanium [25].

Recent studies by Bartkowiak [17] and by Song, Wang, and Mazumder [18], [19] demonstrate the potential utility of OES for monitoring of AM processes. Using powder-blown, direct-energy deposition, Bartkowiak demonstrated that spectral line emissions varied with energy input during deposition of Inconel 625. Also using directed-energy deposition, Song and Mazumder [18] found that analysis of the ratio of specific chromium (Cr I) to iron (Fe I) emission lines could be used to accurately determine chromium concentration in AM of H13 tool steel mixed with 10–60% chromium. Predictions of the chromium concentration using the gaseous plume excitation temperature and electron density were also attempted, though they proved less reliable than the line ratio technique. Further investigations [19], also indicated that phase transformations can be detected using the line ratio technique. These works, along with earlier works on weld-quality monitoring, inspire the use of OES for investigation of metal-based AM.

Here, OES is used to investigate defect detection during AM of Ti-6Al-4V using the Optomec, Inc. LENS process. Preliminary OES data and analysis techniques are presented. It is demonstrated that the line-to-continuum ratio of spectral atomic line emissions can be correlated with the formation and presence of lack-of-fusion defects.

## **2. Experimental Setup**

Additive manufacturing experiments were conducted on an Optomec LENS MR-7 laser-based, directed-energy-deposition system. The LENS system utilized a 500 watt, Ytterbium-doped fiber laser (IPG YLR-500-SM). The laser beam spot size was measured, using a Primes, GmbH FocusMonitor system, to have a second-moment diameter of 1.24 mm at the working distance. As shown in figure 1, a working distance of 9.27 mm was used, as measured from the substrate to four, radially-symmetric powder-delivery nozzles. Centered within the four

powder nozzles was a center-purge nozzle through which a coaxial flow of argon exited onto the substrate.

A custom designed-and-built, sensor-mounting fixture surrounded the laser processing head. The fixture assembly is shown in figure 1. Mounted onto the fixture was a spectrometer fiber with a 400  $\mu\text{m}$  diameter silica core. The opening of the optical fiber was protected with a UV-fused silica window and located 59.7 mm from the melt pool. The viewing angle of the spectrometer was 75 degrees with respect to the laser beam. The opposite end of the optical fiber was coupled to an Ocean Optics, Inc. HR4000 CG UV-NIR spectrometer with a spectral range from 200 to 1100 nm and an optical resolution of 0.50 nm (full width at half maximum). Absolute intensity calibration was not performed on the spectrometer. The spectrometer was synchronized with part buildup, using custom-written software, such that the time, position, layer, and hatch number were all stored with each collected spectrum. A spectrometer integration time of 100 ms and a capture rate of  $8.3\bar{3}$  Hz were used.

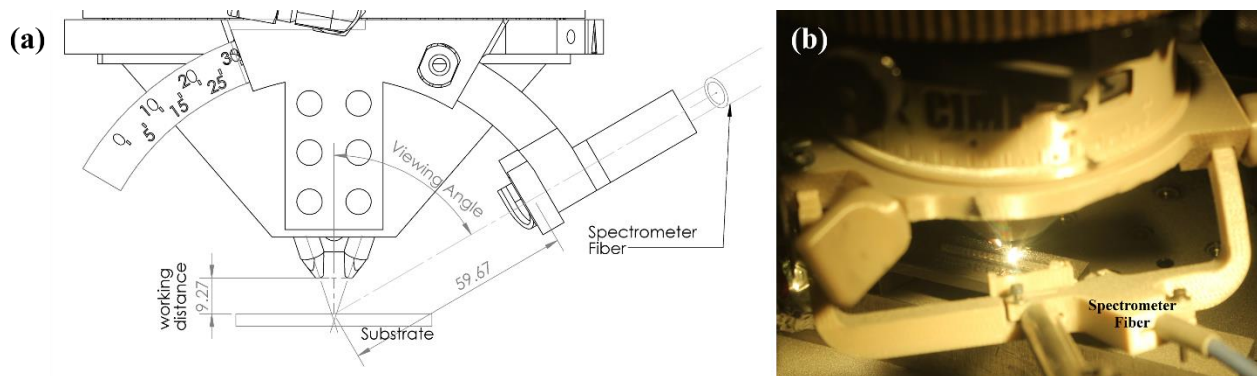


Figure 1: (a) LENS processing head with custom-build, sensor-mounting fixture. (b) Image of fixture, taken during processing, showing spectrometer fiber.

Both the substrate and filler material were ASTM grade 5 titanium (Ti-6Al-4V). The powder was spherical, Extra Low Interstitials (ELI)-grade with a mean particle size distribution of 126.8  $\mu\text{m}$  (stdev = 45.94  $\mu\text{m}$ ). The substrate was 3.175 mm thick and ground-finished. Prior to processing, the substrate was cleaned with acetone and isopropyl alcohol.

Processing was conducted in a positive-pressure, argon-filled chamber, maintained at 2 to 3 inches of water (498 to 748 Pa) gauge pressure. Oxygen was below 20 ppm during processing. Titanium powder flow rates were measured at 3 grams per minute. A measured output laser power of 450 W, and a processing speed of 10.58 mm/s were used for part deposition.

A rectangular block, shown in figure 2, with internally-varying hatch spacing was selected for deposition. The block was built-up using a total of 71 layers spaced 0.173 mm apart. On each layer, a total of thirty-nine parallel hatches were deposited. Each hatch was 3.18 mm

long, extending along the width of the block. As shown in figure 3, the spacing between hatches was increased from 0.914 mm at one end of the block to 1.829 mm at the other. Hatch spacing was incremented by 0.229 mm every ten millimeters.

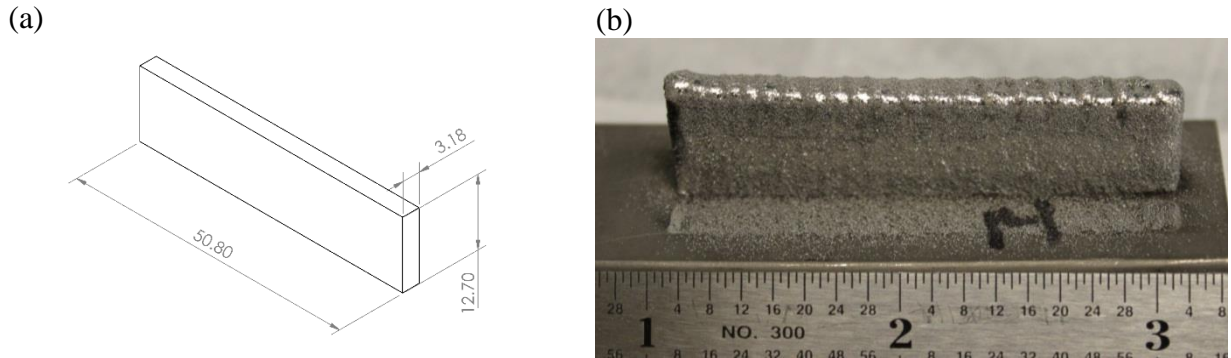


Figure 2: (a) Part geometry with dimensions in millimeters. (b) Image of deposited part.

On each layer, a contour was first deposited along the perimeter of the part, followed by hatches. Hatches were deposited using a zig-zag raster, as shown in figure 3. The order of hatches was unchanged from layer to layer. This geometry was purposely chosen to introduce lack-of-fusion defects between neighboring hatches within the widely-spaced-hatch regions.

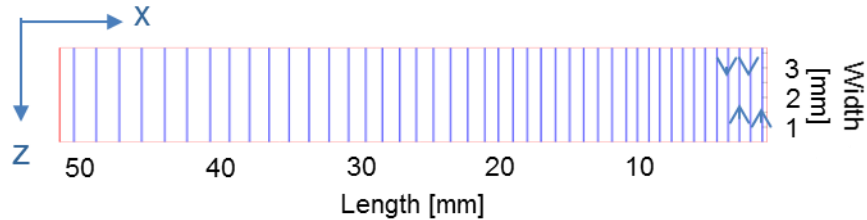


Figure 3: Illustration of deposition path (not to scale). A contour was deposited on each layer followed by hatches starting at the lower right corner of the figure.

After buildup, parts were cross-sectioned through their middle, perpendicular to the hatch vectors, then ground and polished using standard metallographic techniques. Polished cross sections were etched using Kroll's reagent and imaged under an optical-microscope equipped with a digital camera. Computed topography (CT) scans were also taken using a GE phoenix v|tome|x m system using a 300 kV microfocus tube.

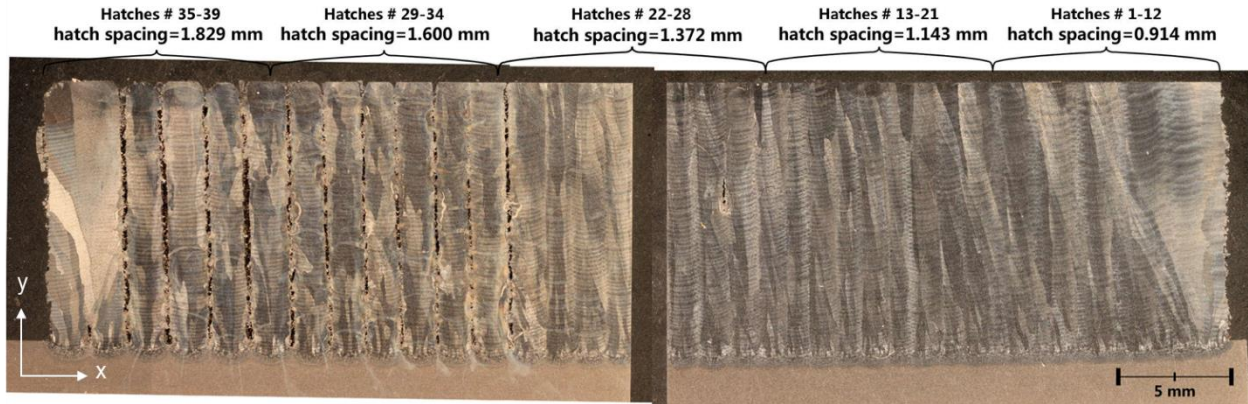


Figure 4: Cross-sectional macrograph of deposited part.

### 3. Results and Data Analysis

A cross-section, taken through the center of the deposit, perpendicular to the hatching vectors (figure 4), revealed internal lack-of-fusion defects between hatches spaced at and above 1.6 mm apart. CT scans of the build (figure 5) confirmed the presence of defects midway through the width of the build. Lack-of-fusion was most prominent for hatches 35 to 39, which were spaced 1.829 mm apart, though defects were also observed at hatches spaced 1.372 mm apart. Based on CT-scans, these lack-of-fusion defects were observed only between hatches and not along the outer contours of the deposit—see figure 5.

Manual observations of collected spectra indicated that spectral emissions attributable to atomic titanium and vanadium emissions were more intense over regions where defects were observed. Optical emissions captured over layer 35, shown in figure 6, illustrate this observation. Line emissions around 625, 550, 520, 500, 453, 445, 430, and 395 nm were most intense throughout the regions with intentional defects, i.e. hatches 19 through 39.

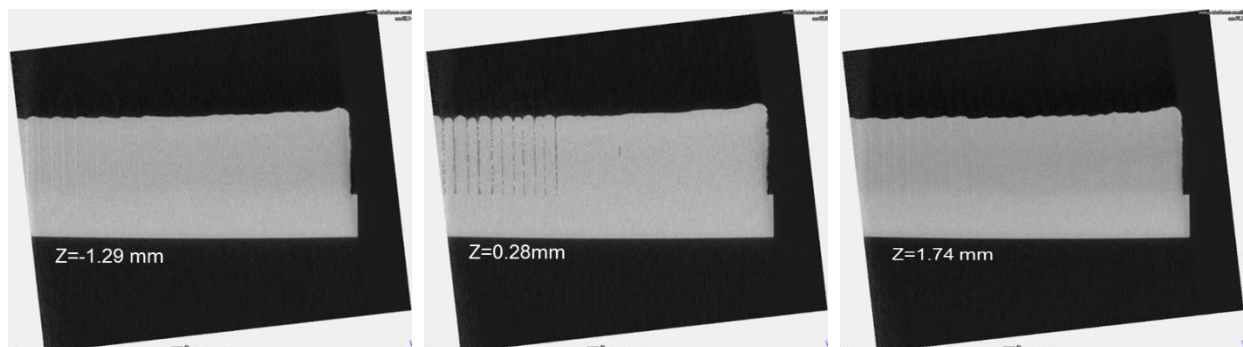


Figure 5: CT-Scans at three locations through the deposit. The center of the deposit was at approximately  $Z=0$  mm.

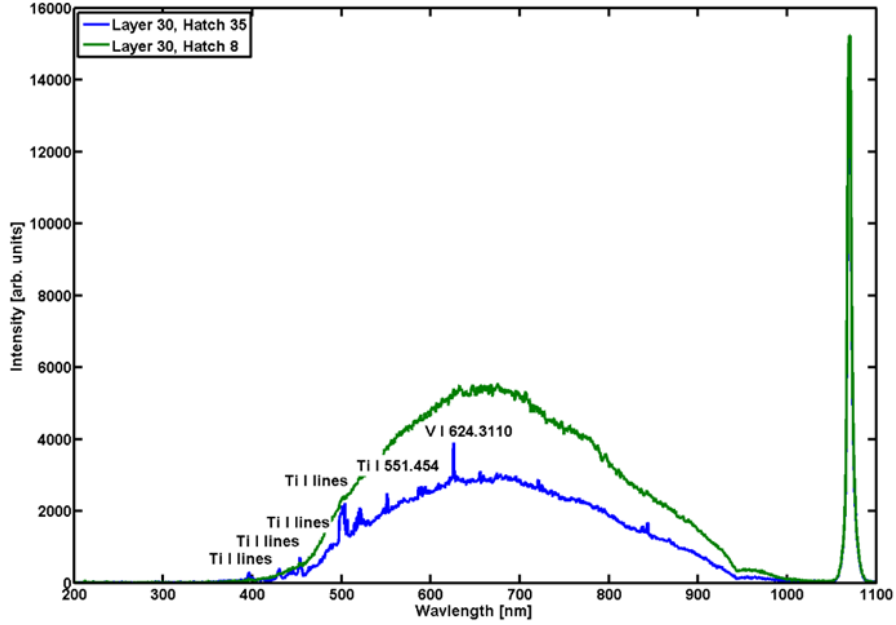


Figure 6: Optical emission spectra captures above hatch 35 (blue) and hatch 8 (green) on layer 30 of the deposit. Atomic emissions of titanium and vanadium were observed over hatch 35, where lack-of-fusion defects were also observed. Note that scattered laser-beam light was observed at 1070 nm.

Based on the observation that line radiation was most prominent over defect regions, a line-to-continuum ratio technique was investigated for correlations with defect location. The continuum radiation was defined according to equation (1),

$$I_{Continuum} = \int_{\lambda_0 - \Delta\lambda}^{\lambda_0 + \Delta\lambda} \frac{I(\lambda_0 + \Delta\lambda) - I(\lambda_0 - \Delta\lambda)}{2\Delta\lambda} \cdot \lambda \, d\lambda + I(\lambda_0 - \Delta\lambda)d\lambda, \quad (1)$$

Where  $I(\lambda)$  is the observed spectral radiation for a wavelength  $\lambda$ ,  $\lambda_0$  is the central wavelength, and  $2\Delta\lambda$  is the wavelength window over which line emissions were observed. Line emissions over the wavelength window was defined according to equation (2),

$$I_{\lambda_0} = \int_{\lambda_0 - \Delta\lambda}^{\lambda_0 + \Delta\lambda} I(\lambda) \, d\lambda - I_{Continuum} \quad (2)$$

An illustration of the line radiation and continuum radiation is provided in figure 7. The line-to-continuum ratio was defined as  $I_{\lambda_0}/I_{Continuum}$ .

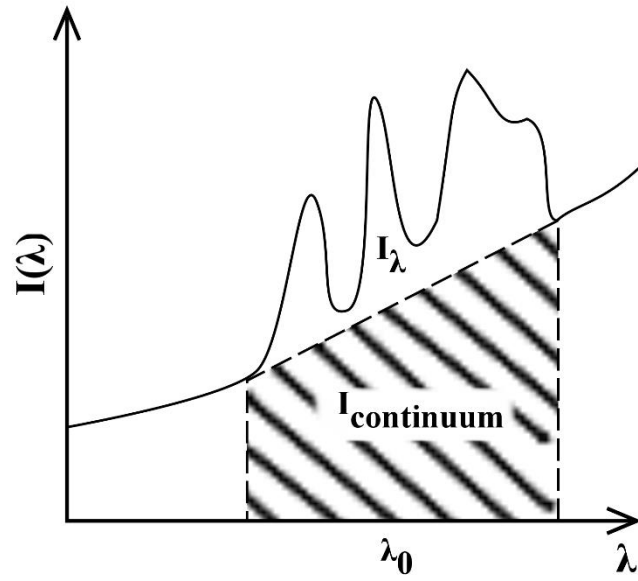


Figure 7: Definition of  $I_{\lambda}$  and  $I_{continuum}$ .

Preliminary analysis of the line-to-continuum ratio was conducted around 550 nm, with a wavelength window of 10 nm and around 430 nm with a wavelength window of 7 nm. Within each region, several overlapping titanium (Ti I) line emission were observed. The spectrometer resolution was insufficient for deconvolution of individual spectral lines. The average line-to-continuum ratio for each region, on layer 30, as a function of hatch number, is shown in figure 8. Around both 430 and 500 nm, the line-to-continuum ratio was lowest for defect-free hatches. Beyond hatch 28, the line-to-continuum ratio values above 0.3 were observed. This indicated the presence of strong line emissions over defect-containing hatches.

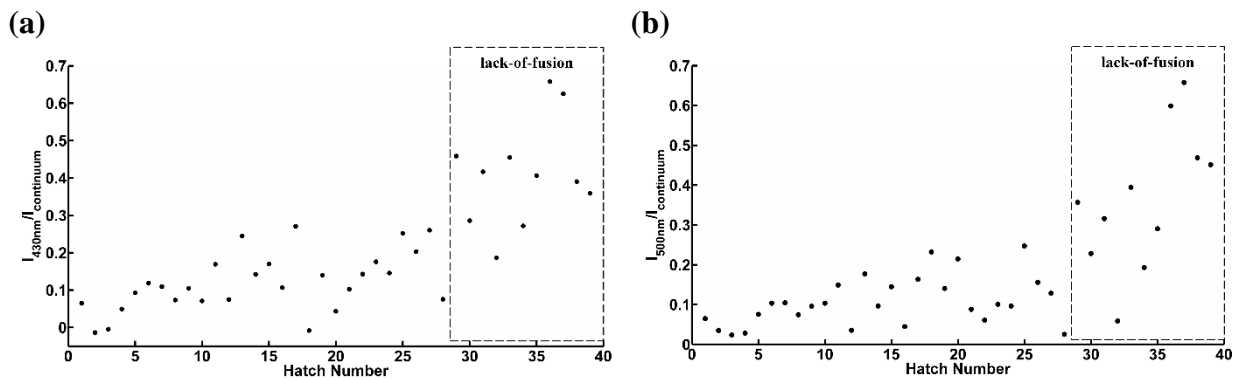


Figure 8: Average line-to-continuum ratio, around (a) 550 nm and (b) 430 nm emission lines, over each hatch of layer 30.

#### **4. Discussion and Concluding Remarks**

Observed optical emission from excited or ionized gases above a substrate are influenced by many factors, including present atomic and molecular species, species concentration, ion, electron and excitation temperatures, and the optical thickness of the plume. These factors are in turn influenced by how the laser interacts with the melt pool, how and which species are vaporized, and interactions of the laser beam with emitted species and with atmospheric gases. Thus, fluctuations in melt pool dynamics or in the surrounding substrate temperature—for example, due to localized heating of an insulated defect—affect the characteristics of excited and ionized gases above the substrate. Given this, optical emission of excited gases and plasma may serve as a proxy for monitoring weld pool, surface, and subsurface conditions during additive manufacturing.

Our results indicate that defects formed as a result of improper parameter section, and possibly melt pool instability, correlated with increased and fluctuating line emissions from excited gases above the melt pool. In the experiments described here, Ti-6Al-4V was deposited atop a Ti-6Al-4V substrate. The line-to-continuum ratio of Ti I emissions around 430 nm and 550 nm were found to correlate with defect locations. Over defect-containing regions, the line-to-continuum ratio fluctuated from hatch to hatch; this may be indicative of instabilities within the excited gases above melt pool during deposition.

Based on this work, we argue that optical emissions sensors may be used for monitoring lack-of-fusion defects between hatches, and instabilities during the additive manufacturing of metals. The extent to which this technique can be applied to monitoring of lack-of-fusion between layers is being explored. Work is also ongoing to explore the potential of applying high-speed camera imaging, photodiodes, and custom-built spectrometers to further explore the line-to-continuum ratio technique, described here, for defect detection. Applications to other metallic systems and other AM processes are also being explored.

#### **Acknowledgements**

The authors acknowledge Dr. David B. Saint John and Mr. Griffin T. Jones for performing computed topography scans of processed samples and Mr. Ed A. Good for help with metallography. This work was supported by the Office of Naval Research, under Contract No. N00014-11-1-0668. Any opinions, findings and conclusions or recommendations expressed in this publication are those of the authors and do not necessarily reflect the views of the Office of Naval Research.

#### **References**

- [1] W. M. Steen and J. Mazumder, “Laser Automation and In-process Sensing,” in *Laser Material Processing*, Springer London, 2010, pp. 485–518.
- [2] M. R. Boddu, R. G. Landers, and F. W. Liou, “Control of laser cladding for rapid prototyping—A review,” in *Solid freeform fabrication symposium Proceedings*, 2001, pp. 6–8.

- [3] E. W. Reutzler and A. R. Nassar, "A review of sensing and control for metal-based additive manufacturing," in *Solid Freeform Fabrication Proceedings*, Austin, TX. (submitted), 2014.
- [4] A. Sun, E. Kannatey-Asibu Jr, and M. Gartner, "Sensor systems for real-time monitoring of laser weld quality," *J. Laser Appl.*, vol. 11, no. 4, pp. 153–168, 1999.
- [5] J. R. Araujo, J. J. Rodriguez-Andina, J. Farina, F. Vidal, J. L. Mato, and M. A. Montealegre, "FPGA-based laser cladding system with increased robustness to optical defects," in *IECON 2012-38th Annual Conference on IEEE Industrial Electronics Society*, 2012, pp. 4688–4693.
- [6] J.-P. Kruth, P. Mercelis, J. Van Vaerenbergh, and T. Craeghs, "Feedback control of selective laser melting," in *Proceedings of the 3rd International Conference on Advanced Research in Virtual and Rapid Prototyping*, 2007, pp. 521–527.
- [7] G. Bi, B. Schürmann, A. Gasser, K. Wissenbach, and R. Poprawe, "Development and qualification of a novel laser-cladding head with integrated sensors," *Int. J. Mach. Tools Manuf.*, vol. 47, no. 3–4, pp. 555–561, Mar. 2007.
- [8] J. T. Hofman, B. Pathiraj, J. van Dijk, D. F. de Lange, and J. Meijer, "A camera based feedback control strategy for the laser cladding process," *J. Mater. Process. Technol.*, vol. 212, no. 11, pp. 2455–2462, Nov. 2012.
- [9] D. Hu, H. Mei, and R. Kovacevic, "Closed loop control of 3d laser cladding based on infrared sensing," in *Solid Freeform Fabrication Proceedings*, 2001, pp. 129–137.
- [10] G. Bi, A. Gasser, K. Wissenbach, A. Drenker, and R. Poprawe, "Identification and qualification of temperature signal for monitoring and control in laser cladding," *Opt. Lasers Eng.*, vol. 44, no. 12, pp. 1348–1359, Dec. 2006.
- [11] L. Song and J. Mazumder, "Feedback control of melt pool temperature during laser cladding process," *Control Syst. Technol. IEEE Trans. On*, vol. 19, no. 6, pp. 1349–1356, 2011.
- [12] D. P. Hand, M. D. T. Fox, F. M. Haran, C. Peters, S. A. Morgan, M. A. McLean, W. M. Steen, and J. D. C. Jones, "Optical focus control system for laser welding and direct casting," *Opt. Lasers Eng.*, vol. 34, no. 4, pp. 415–427, 2000.
- [13] A. Fathi, A. Khajepour, E. Toyserkani, and M. Durali, "Clad height control in laser solid freeform fabrication using a feedforward PID controller," *Int. J. Adv. Manuf. Technol.*, vol. 35, no. 3–4, pp. 280–292, Oct. 2006.
- [14] M. Zeinali and A. Khajepour, "Height Control in Laser Cladding Using Adaptive Sliding Mode Technique: Theory and Experiment," *J. Manuf. Sci. Eng.*, vol. 132, no. 4, p. 041016, 2010.
- [15] A. Heralić, A.-K. Christiansson, and B. Lennartson, "Height control of laser metal-wire deposition based on iterative learning control and 3D scanning," *Opt. Lasers Eng.*, vol. 50, no. 9, pp. 1230–1241, Sep. 2012.
- [16] L. Song, V. Bagavath-Singh, B. Dutta, and J. Mazumder, "Control of melt pool temperature and deposition height during direct metal deposition process," *Int. J. Adv. Manuf. Technol.*, vol. 58, no. 1–4, pp. 247–256, May 2011.
- [17] K. Bartkowiak, "Direct laser deposition process within spectrographic analysis in situ," *Phys. Procedia*, vol. 5, pp. 623–629, Jan. 2010.
- [18] L. Song and J. Mazumder, "Real Time Cr Measurement Using Optical Emission Spectroscopy During Direct Metal Deposition Process," *IEEE Sens. J.*, vol. 12, no. 5, pp. 958–964, May 2012.

- [19] L. Song, C. Wang, and J. Mazumder, "Identification of phase transformation using optical emission spectroscopy for direct metal deposition process," 2012, p. 82390G–82390G–9.
- [20] A. Ancona, V. Spagnolo, P. M. Lugara, and M. Ferrara, "Optical Sensor for real-time Monitoring of CO<sub>2</sub> Laser Welding Process," *Appl. Opt.*, vol. 40, no. 33, pp. 6019–6025, 2001.
- [21] T. Sibillano, A. Ancona, V. Berardi, E. Schingaro, G. Basile, and P. Mario Lugarà, "A study of the shielding gas influence on the laser beam welding of AA5083 aluminium alloys by in-process spectroscopic investigation," *Opt. Lasers Eng.*, vol. 44, no. 10, pp. 1039–1051, Oct. 2006.
- [22] M. M. Collur and T. DebRoy, "Emission spectroscopy of plasma during laser welding of AISI 201 stainless steel," *Metall. Mater. Trans. B*, vol. 20, no. 2, pp. 277–286, 1989.
- [23] Z. Szymanski, J. Kurzyna, and W. Kalita, "The spectroscopy of the plasma plume induced during laser welding of stainless steel and titanium," *J. Phys. Appl. Phys.*, vol. 30, no. 22, p. 3153, 1997.
- [24] P. Sforza and D. de Blasiis, "On-line optical monitoring system for arc welding," *NDT E Int.*, vol. 35, no. 1, pp. 37–43, Jan. 2002.
- [25] A. R. Nassar, R. Akarapu, S. M. Copley, and J. A. Todd, "Investigations of laser-sustained plasma and its role in laser nitriding of titanium," *J. Phys. Appl. Phys.*, vol. 45, no. 18, p. 185401, May 2012.